Dichloroacetate improves hepatic and systemic energy metabolism during sepsis

Rabina Mainali[1*], Manal Zabalwi[2*], David Long[2], Nancy Buechler[1], Shalini Jain[3], Ellen Quillen[2], Chia-Chi Key[2], Xuewei Zhu[2], Peter W. Stacpoole[4], Jennifer Martinez[5], Charles E. McCall[2#], Matthew A, Quinn[1,2,5#]

[1]Department of Pathology, Section on Comparative Medicine Wake Forest School of Medicine, Winston-Salem, North Carolina

[2]Department of Internal Medicine, Section of Molecular Medicine Wake Forest School of Medicine, Winston-Salem, North Carolina

[3]Department of Internal Medicine, Section of Endocrinology and Metabolism Wake Forest School of Medicine, Winston-Salem, North Carolina

[4]Division of Endocrinology, Diabetes and Metabolism and Department of Biochemistry and Molecular Biology, University of Florida College of Medicine, Gainesville, Florida

[4]Immunity, Inflammation, and Disease Laboratory, National Institute of Environmental Health Sciences (NIEHS), National Institutes of Health (NIH), Research Triangle Park, NC

[5]Lead Contact

* these authors contributed equally
# denotes co-corresponding author

Corresponding Authors:

Matthew A. Quinn, Ph.D.
Wake Forest School of Medicine
Medical Center Blvd
Winston-Salem, NC 27157
Office: 336-713-1995
mquinn@wakehealth.edu

Charles E. McCall, M.D.
Wake Forest School of Medicine
Medical Center Blvd
Winston-Salem, NC 27157
Office: 336 413 8034
chmccall@wakehealth.edu

Keywords: sepsis, mitochondria function, liver, inflammation, metabolism, steatosis

Abstract

Dramatic metabolic reprogramming between an anabolic resistance and catabolic tolerance occurs within the immune system in response to systemic infection with the sepsis syndrome. While metabolic tissues such as the liver are subject to end-organ damage during sepsis and are the primary cause of sepsis death, how their metabolic and energy reprogramming during sepsis state ensures survival is unclear. Employing comprehensive metabolomic screening, targeted lipidomic screening, and transcriptional profiling in a mouse model of septic shock, we show that hepatocyte lipid metabolism, mitochondrial TCA energetics, and redox balance are significantly reprogramed after cecal ligation and puncture (CLP). We identify increases in TCA cycle metabolites citrate, cis-aconitate, and itaconate with reduced fumarate, elevated triglyceride synthesis, and lipid droplet accumulation in the septic hepatocytes. Transcription analysis of liver tissue supports and extends the hepatocyte findings. Plasma metabolomics show systemic hypoglycemia and increased concentrations of free fatty acids, ketones and corticosterone in parallel with liver reprogramming. Strikingly, the administration of the pyruvate dehydrogenase kinase (PDK) inhibitor dichloroacetate (DCA) reverses dysregulated hepatocyte and systemic metabolism and mitochondrial dysfunction. DCA administered during sepsis arrests anorexia and weight loss, restores V02 levels as an index of increased carbohydrate oxidation and promotes physical activity. We suggest that sepsis inflicts an energy demand and supply crisis with distinct shifts in hepatocyte and systemic mitochondrial function. Targeting the mitochondrial PDC/PDK energy homeostat rebalances life-threatening energy deregulation caused by bacterial sepsis.

Introduction

Sepsis represents a life-threatening condition that results from dysregulated inflammatory responses to disseminated and uncontrolled infection. If not diagnosed and treated early after its onset, sepsis may limit survival by inducing early shock and subsequent immunometabolic paralysis. Sepsis accounts for one in three hospital deaths in the U.S. and millions of deaths each year globally, highlighting its hazard to public health [1,2]. The high mortality rate associated with sepsis reflects the lack of a clinically viable molecular-based therapeutic target. Therefore, understanding the pathogenesis of sepsis at both the molecular and organismal levels is major gap in public health and of the utmost importance.

Sepsis is a biphasic phenomenon, with clearly defined acute and chronic phases [3,4]. The acute phase of sepsis is driven by high energy consumption and hyper-inflammation characterized by oxidative stress, followed by cellular reprogramming to a low energy, anti-inflammatory state of immunometabolic paralysis, with accompanying organ failure.[2,5]. In addition to inflammatory responses, dysregulation of the host's metabolism during sepsis plays a vital role in its progression and severity [6-8]. Compared to healthy individuals, energy homeostasis is significantly altered in septic patients [7,8]. The early phase of sepsis is a hypermetabolic condition marked by increased catabolism of fats, proteins and carbohydrates, associated with high rates of oxygen consumption and ATP synthesis [9-11]. Following the acute phase is a hypometabolic state where ATP production and mitochondrial respiration decrease [9]. Immune cells and some organ cells enter an energy

86 conserving “hibernation-like” state as a protective mechanism to lower the metabolic de-
87 mands of the cell and help with its recovery [6,12,13]. However, staying in this hypometabolic
88 state for a prolonged period can lead to organ dysfunction and failure [12,13].

89 Of particular interest is that, during the hyper-inflammatory anabolic phase of sep-
90 sis, an increase in the expression and activity of pyruvate dehydrogenase kinase 1
91 (PDK1) consistently occurs [4]. This enzyme is one of four PDK isoforms that reversibly
92 phosphorylates serine residues on pyruvate dehydrogenase complex (PDC) E1α subunit,
93 inhibiting the conversion of pyruvate to acetyl coenzyme A (acetyl CoA) [14]. Inhibition of
94 this important enzymatic activity that connects glycolysis to tricarboxylic cycle (TCA), ox-
95 idative phosphorylation (OXPHOS) and the lipogenic pathway is thought to be one of the
96 main mechanisms that is driving dysfunction of mitochondrial respiration and cell bioen-
97 ergetics observed during sepsis [15,16], suggesting that PDK may be a novel, druggable
98 target for treatment of sepsis..

99 There a few reports that indicate changes in hepatic metabolism during sepsis but
100 these studies are not conclusive [17]. Therefore, there is limited knowledge regarding the
101 metabolic changes and infection related liver dysfunction in response to sepsis. There-
102 fore, we set out to characterize the global hepatic manifestations of sepsis, with the over-
103 all goal of identifying master regulators of the hepatic metabolic response to polymicrobial
104 infection.

105

106

107

108

Results

Sepsis Impairs Hepatic Mitochondrial Metabolism

To test the long-term hepatic transcriptional changes elicited by sepsis we performed RNA-seq in whole livers thirty-hours post cecal ligation puncture (CLP). At this time point, septic mice exhibit tolerance, in which immunometaboic paralysis and end organ dysfunctions decrease survival. Ingenuity pathway analysis (IPA) of the top physiological pathways subject to alteration in response to sepsis revealed a significant increase in the acute phase response pathway, highlighting a persistent inflammatory state in the liver into the chronic phase of sepsis (Fig. 1a). Of particular interest were the findings that oxidative phosphorylation and mitochondrial dysfunction were the top two enriched pathways in the liver of septic mice (Fig. 1a). To gain further insight into the effects of sepsis on the transcriptional regulation of mitochondrial function we performed gene set enrichment analysis (GSEA) of the oxidative phosphorylation pathway (GO:0006119). Septic mice at 30 h decreased the transcriptional output of OXPHOS components, as evidenced by a negative GSEA enrichment score (Fig. 1b). Given the connection between oxidative phosphorylation and the tricarboxylic acid (TCA) cycle, we next asked if polymicrobial infection would elicit similar alterations in this pathway. In accordance with the changes observed in the oxidative phosphorylation pathway, we found a negative enrichment score for TCA cycle enzymes (GO:0006099) in the liver of CLP mice (Fig. 1c). Thus, our transcriptome data indicate that sepsis impairs mitochondrial metabolism in the liver.

Next we wanted to assess if the transcriptional changes elicited by sepsis would manifest in altered hepatic TCA cycle metabolism. Therefore, we performed global

133 unbiased metabolomic screening in isolated hepatocytes from control and septic mice by
134 Ultrahigh Performance Liquid Chromotography-Tandem Mass Spectroscopy (UPLC-
135 MS/MS). In line with altered transcriptional regulation of the TCA cycle, we found that
136 sepsis altered the relative abundance of multiple metabolites involved in the TCA cycle
137 (Fig. 1d). In particular, significant elevation of citrate and cis-aconitate was observed in
138 septic hepatocytes at 30h (Fig. 1e&f). Unlike macrophages, which shift their ratio of
139 succinate and α-ketoglutarate to favor succinate accumulation over α-ketoglutarate [18-20],
140 we found no changes in the levels of these metabolites in hepatocytes (Fig. 1G&H).
141 Furthermore, unlike macrophages [21], levels of fumarate decreased, but malate levels
142 were unchanged in hepatocytes from septic animals (Fig. 1I&J). Monocytes,
143 macrophages and dendritic cells reprogram the TCA cycle during acute inflammation to
144 a catabolic tolerance phenotype by shunting cis-aconitate to itaconate through the
145 enzymatic action of aconitase decarboxylase (ACOD1; also known as immune
146 responsive gene 1 [IRG1]) [21-24]. Accordingly, we also found that sepsis significantly
147 induces *ACOD1* and elevates itaconate in isolate hepatocyte preparations (Fig. 1K&L).
148

149 **Sepsis Impairs Hepatic Redox Balance and Promotes Oxidative Stress**

150 Perturbations in oxidative phosphorylation have been shown to promote the
151 production of reactive oxygen species (ROS) [25]. Furthermore, itaconate has been shown
152 to induce genes involved in oxidative stress regulation through activation of the master
153 NRF2 KEAP1 antioxidative pathway in macrophages [23]. Therefore, we examined if sepsis
154 invokes a gene expression profile involved in regulation of ROS. GSEA of the ROS
155 metabolic process pathway (GO:0072593) revealed a positive enrichment, highlighting

156 the transcriptional induction of genes involved in the regulation of oxidative stress in livers
157 of septic mice (Fig. 2a). Given the induction of ROS metabolic genes we wanted to
158 determine if sepsis alters key metabolites involved in redox balance, specifically the
159 cysteine-glutathione transsulfuration redox regulatory cycle. Hepatocytes isolated during
160 sepsis-induced tolerance did not adjust intracellular homocysteine levels (Fig. 2b),
161 however, cystathionine significantly decreased (Fig. 2c). Furthermore, we found a trend
162 for decreased cysteine levels in the liver (p=0.0534) (Fig. 2d) and significantly decreased
163 glycine (Fig. 2e). Most dramatically, septic mice depleted hepatocyte glutathione (Fig. 2f).
164 During oxidative stress, the pool of glutathione shifts from reduced glutathione (GSH) to
165 oxidized glutathione (GSSG). Additional evidence of increased hepatic oxidative stress
166 was a significant shift in the cellular glutathione pools, favoring GSSG over GSH in CLP
167 mice compared to sham controls (Fig. 2g).
168

169 **Sepsis promotes hepatic steatosis**

170 Thus far, our data revealed that sepsis induces significant impairments in hepato-
171 cyte OXPHOS, alterations in the TCA cycle, and induction of oxidative stress, findings
172 that are also metabolic hallmarks of fatty liver disease [26]. Because perturbations in global
173 lipid profiles occur in septic patients [11], we evaluated the effects of CLP on the hepatic
174 lipid metabolism pathway. In support of our hypothesis that sepsis alters hepatic lipid
175 metabolism, transcriptome data indicate significant repression of lipid metabolism in livers
176 of septic mice (Fig. 3a). Sepsis also decreased transcription output that supports fatty
177 acid metabolic process components in the liver, as evidenced by a negative GSEA en-
178 richment score (Fig. 3b).

179 Since hepatic lipid metabolism significantly changes during sepsis, we further in-
180 vestigated the effect of sepsis on both the fatty acid oxidation and biosynthetic processes
181 pathways. Slight changes occurred in the expression profiles of genes involved in fatty
182 acid oxidation in response to CLP after 30 h. In contrast, we found a striking increase in
183 genes involved in fatty acid biosynthesis (Fig. 3c). We then asked whether the transcrip-
184 tional alterations elicited by sepsis would be manifested in hepatic lipid metabolites. Con-
185 sistent with our transcriptional profiling, our unbiased metabolomic screening in hepato-
186 cytes identified lipid metabolism as the top metabolic pathway altered in sepsis (Fig.3d).
187 Our metabolomic screen identified increases in virtually all fatty acids and acylcarnitine
188 derivatives assayed (Fig. 3e). Given the consistency between our transcriptome data and
189 metabolomics panel, we performed lipidomic screening in the liver of sham vs CLP mice
190 to capture the global consequences of sepsis on hepatic lipid metabolism. Strikingly, we
191 find over 500 lipid species increased in septic hepatocytes (Fig.3f). As a consequence of
192 alterations in lipid metabolism, we observe an increase in lipid droplet formation in liver
193 tissues of CLP mice (Fig. 3g), confirming the presence of hepatic steatosis.
194

195 **Sepsis-induced anorexia increases plasma free fatty acids**

196 The onset of anorexia and a switch from glucose metabolism to alternative fuel
197 sources during sepsis has been well established [11,27,28]. Consistent with this principle [29],
198 septic mice housed in metabolic chambers exhibited onset of anorexia, as evidenced by
199 a marked decrease in total food intake (Fig. 4a). While anorexia induced by systemic
200 inflammation is highly conserved, the extent to which sepsis-associated anorexia is as-
201 sociated with altered plasma metabolites is unclear. To address this knowledge gap, we

202 performed global metabolomic screen in plasma from sham and CLP mice 30 hours post-
203 surgery. We find plasma metabolites known to be altered in the fasting state are indeed
204 altered in response to polymicrobial infection. Specifically, sepsis induces a significant
205 decrease in the relative abundance of plasma glucose compared to sham mice (Fig. 4b).
206 Similar to previous reports [30], increased circulating levels of corticosterone, a primary
207 mediator of the fasting response also occurred (Fig. 4c). During nutrient deprivation, ke-
208 togenesis increases circulating ketones [31]. Likewise, we found elevated levels of circulat-
209 ing ketone bodies 3-hydroxybutyrate, 2-hydroxybutyrate, and 2-aminobutyric in septic
210 mice (Fig. 4d-f). (Fig. 4d-f). Fasting also liberates free fatty acids and increases their
211 levels in plasma [32]. Consistent with a fasting response, sepsis increased 75 lipid species
212 in the circulation (Fig. 4g). Collectively, these data indicate sepsis induces a systemic
213 starvation state, concomitant with repressed mitochondrial energetics and nutrient
214 changes in hepatocytes.

215

216 **PDK inhibition attenuates sepsis-induced transcriptional and metabolic changes**
217 **in the liver**

218 Given the establishment of hepatocyte mitochondrial dysfunction and steatosis
219 during sepsis, we asked whether pharmacological targeting of the hepatic PDK/PDC axis
220 would mitigate the disruption of key metabolic and bioenergetic processes induced by
221 sepsis. We previously reported that PDK inhibition by the pyruvate analog and pan-PDK
222 inhibitor dichloroacetate (DCA) promotes PDC-dependent immunometabolic adaptations
223 to sepsis and increases survival [15,33]. Therefore, we hypothesized that PDK inhibition

224 would also ameliorate sepsis-induced metabolic dysfunction in the liver. To test this pos-
225 tulate, we administered DCA to septic mice 24 h after CLP onset and assessed the global
226 transcription profile of liver 6 h later via RNA-seq. DCA treatment of septic mice reversed
227 the majority of sepsis-regulated gene networks (Fig. 5a). DCA also restored to nearly
228 sham levels the top physiological pathways altered in response to sepsis, such as inflam-
229 mation mediators, lipid triglycerides synthesis, redox control and mitochondrial TCA func-
230 tion (Fig. 5b).

231 Given our reversal of the sepsis-regulated hepatic transcriptome by DCA, we next
232 determined whether it would have functional effects on the hepatic metabolome. We re-
233 peated our unbiased metabolomic profiling in isolated hepatocytes from septic mice and
234 found that TCA metabolites that accumulate in hepatocytes during sepsis— citrate, cis-
235 aconitate, and itaconate—returned almost to sham levels after DCA treatment (Fig. 5c).
236 Of particular note, we also observed that DCA treatment did not restore fumarate levels,
237 but rather decreased this TCA intermediate decreased even further than measured in
238 septic livers not exposed to the drug (Fig. 5c).

239 Next, we focused on metabolites proximal to the glutathione synthesis redox path-
240 way, given the transcriptional reversal of the conjugation to glutathione pathway in DCA
241 treated septic mice and distal to methionine (Fig. 5b). We found that DCA not only caused
242 a reversal of cystathionine and taurine low levels in septic mice, but also increased accu-
243 mulation of these metabolites in the liver after DCA (Fig. 5d). No significant differences
244 occurred in glycine. The increased levels of transsulfuration redox metabolites in DCA-
245 treated mice resulted in a reduced oxidative burden in hepatocytes during sepsis, as ev-
246 idenced by an increased GSSG/GSH ratio (Fig. 5e).

247 Finally, given the pronounced steatotic phenotype present during sepsis, and the
248 restoration of mitochondrial function and redox balance in response to DCA treatment,
249 we next determined whether PDK inhibition would also reverse the fatty liver phenotype
250 of sepsis. Metabolomics revealed broad reductions in hepatic mono-, di- and triglycerides
251 in septic mice treated with DCA (Fig. 5f), indicating that PDK activation can control the
252 development of hepatic steatosis during sepsis (Fig. 5g).

253

254 **DCA rescues systemic energy crisis during polymicrobial infection**

255 The above findings strongly suggest that PDK inhibition reverses many sepsis-
256 induced metabolic and transcriptional changes in the liver. We next investigated the sys-
257 temic effects of DCA treatment on energy metabolism in CLP mice. Plasma metabolite
258 screening in CLP mice revealed alterations in over 250 metabolites in response to CLP,
259 with the majority of these metabolites decreasing after DCA treatment (Fig. 6a&b). When
260 we further examined the 198 sepsis-dysregulated metabolites normalized by DCA treat-
261 ment, we found that the majority involve pathways of glycine and methionine metabolism
262 that fuel glutathione (Fig. 6c) and promote the tolerant and antioxidant catabolic phase of
263 sepsis [10]. Consistent with our findings in livers from septic mice, these data indicate that
264 DCA restores circulating metabolite levels comparable to concentrations measured in
265 sham controls and identify a reversal in sepsis-induced systemic energy depletion follow-
266 ing PDK inhibition.

Given that DCA restores levels of sepsis-dysregulated circulating metabolites, we hypothesized that PDK inhibition might also reverse the sepsis-induced anorexia response and starvation. To test this hypothesis, we housed septic mice treated with or without DCA in metabolic cages for after sepsis onset. Consistent with previous reports [34-36], CLP induced a dramatic decrease in body weight within 24 h of surgery (Fig. 6d). Strikingly, DCA administration completely normalized body weight in septic mice (Fig. 6d) and increased physical activity (data not shown). DCA-induced body weight correction may result from decreasing anorexia, as food intake concomitantly increased in DCA-treated septic mice (Fig. 6e). While modestly increases in respiratory exchange ratio (RER) occurred, DCA restored VO2 to sham values. We interpret the VO2 increase as indicating that PDK inhibition readjusts carbohydrate oxidation during sepsis starvation, consistent with PDC activation (Fig. 6f&g). Together, our findings identify PDK as a significant driver of systemic energy imbalance during sepsis and a therapeutic target for its reversal by increasing PDC oxidation of glucose carbons. Contributing to this effect are reversing anorexia, increasing food intake and restoring mitochondrial function (Fig. 6h).

297 **Discussion**

298

299 Considerable attention has been focused recently on the immunometabolic
300 consequences of inmflammation in immune cells [37]. However, significant gaps exist in our
301 understanding of the metabolic adaptations induced by systeminc inflammation from
302 sepsis in vital organs. Addressing this limitation is critical because sepsis survival
303 depends on restoring both organ and immune cell homeostasis following dysregulated
304 and disseminated inflammation [13]. The present study reveals major disruption of several
305 key aspects of hepatic mitochondrial metabolic and bioenergy functions in septic mice,
306 including TCA cycle activity, OXPHOS, redox balance and lipid metabolism. In addition,
307 at the organismal level, anorexia increase as an early response to sepsis followed by an
308 altered circulating lipid profile and increased levels of corticosterone, a pattern consistent
309 with a state of fasting or starvation. Importantly, PDK inhibition by DCA highlights the
310 PDK/PDC as a critical gatekeeper of energy metabolism during life-threatening systemic
311 infection. Within one hour of its administration, DCA reversed the starvation phenotype
312 and, within six hours, restored overall mitochondrial capacity to meet the demands used
313 to regenerate immune and organ physiologic competence. Overall, these findings support
314 the notion that dysregulated mitochondrial reprogramming in hepatocytes contributes to
315 a sepsis-induced systemic energy supply and demand crisis and the vunlerability of PDC
316 to significant post-transcriptional inhibition during sepsis.

317 Upregulation of PDKs inactivates PDC to skew carbohydrate metabolism away
318 from mitochondrial oxidation and promotes cytoplasmic reduction of glycolytically-derived
319 pyruvate to lactate, as the central feature of the Warburg response. Upregulating oxida-
320 tive phosphorylation also shifts immune cells to Warburg glycolysis during cell activation

321 [8,38], and alters levels of TCA cycle citrate, cis-aconitate, succinate, and fumarate metab-
322 olite signaling properties [8,20,38,39]. For example, succinate primes inflammation through
323 succinate dehydrogenase (SDH)-mediated ROS generation and ATP synthesis [20,38].
324 SDH-derived ROS enhances IL-1β production by activating HIF-1α and activating the
325 NLRP3 inflammasome [20]. Inhibition of SDH activity increases IL-10 production and skews
326 inflamed immune cells towards an anti-inflammatory response [20]. Fumarate, on the other
327 hand, possesses anti-inflammatory properties as it inhibits pro-inflammatory cytokine pro-
328 duction either by activating the NRF2 pathway or via inhibiting pathways like NF-κB and
329 MAPK that lie downstream of TLR signaling in immune cells [40,41]. Decreased fumarate
330 did not align with succinate in hepatocytes at the time point assayed.

331 Cis-aconitate decarboxylation to itaconate represses glycolysis [22,42] and dampens
332 inflammation in monocytes and macrophages [21,23]. In response to LPS stimulation,
333 macrophages significantly upregulate IRG1 and accumulate itaconate. Direct inhibition of
334 SDH by itaconate limits IL-1β levels [20]. Transcriptional regulation of the NRF2/Keap1 and
335 IκBζ-ATF3 pathways by itaconate also mute IL-1β expression [23,43,44]. In line with what
336 occurs in macrophages, we observed an increase in IRG1, citrate, cis-aconitate, and
337 itaconate in septic hepatocytes at 30 h. While we did not fully characterize the hepatic
338 function of itaconate, a recent paper demonstrates its anti-inflammatory effects during
339 Ischemia-reperfusion (IR) injury in the liver [45]. The deletion of IRG1 heightens
340 inflammation and liver damage and renders hepatocytes susceptible to oxidative injury
341 after I/R injury. Further, itaconate administration reduces liver damage and inflammation
342 associated with I/R in IRG1 KO mice, also emphasizing its anti-inflammatory and
343 hepatoprotective effects [45]. Given the immunomodulatory effects of itaconate and its

344 accumulation in the liver in our study, we hypothesize that itaconate directs hepatocyte
345 shifts in both TCA cycle metabolism and mitochondrial energetics. DCA reduces itaconate
346 levels, which we also find in a human monocyte model of sepsis [16].

347 ROS also may direct hepatic responses to sepsis . Similar to immune cells, liver
348 cells increase ROS production during sepsis [46,47]. We found that the thiol antioxidant
349 glutathione decreased, concomitant with an increase in oxidized glutathione, in
350 hepatocytes during sepsis. Overall, our findings support the notion that sepsis disrupts
351 hepatic redox balance, as reflected in alterations in glycine, cystathionine and taurine
352 levels in the liver.

353 Sepsis also profoundly alters lipid metabolism, resulting in significant fatty acid
354 and glycerol metabolic shifts in plasma, changes reported to predict prognosis in septic
355 patients [48]. Sirt1 and Sirt6 NAD-dependent deacetylases play an essential role in
356 regulating the balance between glycolysis and fatty acid oxidation [49]. Specifically, Sirt1
357 upregulates PGC-1-dependent fatty acid oxidation during the shift from the acute to the
358 late phase of sepsis. However, we do not observe a fatty acid oxidation transcription
359 profile in septic livers. Yet another vital lipid metabolic pathway in immune cells is *de novo*
360 lipogenesis [50]. Macrophages generate malonyl-CoA and subsequent malonylation of
361 glycolytic enzymes [51]. While we did not measure malonyl-CoA and acetyl-CoA levels, our
362 metabolomics screening did show an increase in hepatic citrate levels. Furthermore, our
363 transcriptional studies identify a cohort of genes in livers from septic animals that are
364 involved in fatty acid biosynthesis. Our data are consistent with human data where
365 patients who died from sepsis had evidence of hepatic steatosis affecting 5%-80% of liver

366 parenchyma [52]. These data emphasize the robust steatotic phenotype conserved
367 between mice and humans.

368 The combination of anorexia and weight loss is an important clinical manifestation
369 of sepsis in humans. Representative animal models demonstrated significant reductions
370 in food intake and body weight in response to infection [11,27,28]. Consistent with a fasting
371 state, we find a circulating metabolomic signature enriched in ketone bodies and
372 glucocorticoids with decreased glucose levels [53-57]. During the fasting period, free fatty
373 acids released from adipose tissues are taken up at a nonsaturable rate by the liver,
374 where they are packaged into triglycerides and transported out and into circulation by
375 very low-density lipoproteins (VLDL), which make them available as an energy source
376 during periods of energy crisis [54,58]. In addition to the fasting metabolomics signature
377 observed in septic mice, we found that sepsis significantly elevates levels of 75 lipid
378 species in the plasma. We propose nutrient depletion as another mechanism contributing
379 to the development of sepsis-induced steatosis.

380 PDC is a master metabolic regulator controlling the conversion of pyruvate to
381 acetyl-CoA in the mitochondria [14] . A part of the metabolic reprogramming that occurs in
382 immune cells in response to inflammatory signaling is inactivation of PDC [14,59]. PDK is a
383 negative regulator of the PDC, as it phosphorylates PDC and inhibits the conversion of
384 pyruvate to acetyl-CoA [14]. During sepsis, the expression and activity of PDK1 in immune
385 cells is heightened, contributing to the dysfunction of mitochondria metabolism. One
386 mechanism driving this observed increase is through pro-inflammatory mediators such as
387 LPS and interferon gamma (IFN-γ) [60]. Another possible mechanism contributing to PDK
388 activation in the context of sepsis is through glucocorticoid signaling [61]. In fact, starvation

389 is well established to activate the PDK pathway [62-66]. Based on our findings of elevated
390 glucocorticoid levels in both the circulation and the liver, we hypothesize the stress
391 hormone pathway as a contributor to PDK activation during sepsis.

392 We reported in a sepsis monocyte model that DCA reduced TCA cycle catabolic
393 effects, concurrent with increasing amino acid anaplerotic catabolism of branched-chain
394 amino acids, leading to increased TCA-driven anabolic energetics [59]. In the present
395 study, we find restoration of TCA metabolites, decreased triglyceride accumulation,
396 lessening of lipid synthesis and oxidative stress rebalances in septic mice after DCA
397 administration. Not only does DCA reverse sepsis-induced gene expressions and
398 metabolic profiles to baseline levels, it also leads to an increase in antioxidants, body
399 weight and food intake, suggesting systemic improvements in response to DCA and
400 reversal of anorexia. Overall we demonstrate that hepatic dysfunction and a systemic
401 energy crisis during sepsis improves after targeting the PDC/PDK axis with DCA.
402 Furthermore, we show sepsis not only affects immunity, but it dysregulates hepatic and
403 organism-wide lipid metabolism and redox homeostasis in the liver. The net results is an
404 energy crisis between low nutrient supply and high energy demand for immunity and
405 organ function.

406 Further work elucidating the mechanistic pathways involved in the dysfunction of
407 lipid metabolism and the impact of TCA metabolite alterations is warranted. In particular,
408 further investigation specifically into the PDK pathway to determine which isoform
409 underlies the hepatic manifestions of sepsis. This is warranted given multiple isoforms of
410 PDK expressed in the liver [67] and DCA inhibits multiple isoforms of PDK [68,69]. The results
411 of this study fill a gap in understanding how sepsis at the molecular level compromises

liver function. It also further informs the novel therapeutic targeting potential of the PDC/PDK homeostat.

Material and Methods

Animal Experiments

Male C57BL/6J mice aged 8-10 weeks were purchased from The Jackson Laboratory (Bar Harbor, ME). All animals were subject to a 12:12 hour dark/light cycle with *ad libitum* access to standard rodent chow and water. Cecal ligation puncture model was used to induce sepsis as previously described [33,70]. Briefly, cecum was ligated and punctured two times with a 22-gauge needle. Contents were then returned and incision was closed in two layers (peritoneum and skin). Sham operation where abdominal incision was made but cecum not ligated or punctured was used as a control. Subcutaneous fluids (1ml normal saline) were given to each animal. Mice were euthanized 30 hours post-surgery for tissue collection. Dichloroacetate (DCA) (Sigma; MO, USA) was administered (25mg/kg) intraperitoneally at various time points post-surgery: for metabolomic screening and RNA-seq DCA was administered 24 hours post-surgery and tissues collected 6 hours post DCA administration (30 hours post-surgery), for metabolic cages DCA was administered immediately post-surgery.

Hepatocyte Isolation

Hepatocytes were isolated via portal vein perfusion and collagenase digestion as previously described [71]. Following perfusion, liver cells were liberated by gentle dissocation in DMEM (ThermoFisher; CA, USA). Cells were then filtered through nylon mesh to remove cellular debris and connective tissue and resulting cells pelleted by centrifugation at 50g for 1 minute. After three washes with DMEM cells were counted and viability assessed via Trypan Blue exclusion.

464

465 **RNA-sequencing**

466 RNA was isolated from whole liver tissues using Trizol and the RNeasy RNA isolation kit
467 (Qiagen; MD, USA) according to manufacturer's protocol. One microgram of high quality
468 RNA (RIN>8) was used as a template for library generation using the Illumina TruSeq
469 RNA Sample Prep Kit v2 (Illumina; CA, USA) according to the manufacturer's protocol.
470 Generated libraries were then poly(A) enriched for mRNA prior to sequencing. Indexed
471 samples were sequenced at 100bp-paired-end protocol with the NovaSeq 6000
472 (Illumina), generating approximately 20-30 million reads per sample. Sequenced reads
473 were aligned to the University of California Santa Cruz (UCSC) mm10 reference genome
474 using STAR v2.5 as previously described [72]. The mapped read counts were quantified by
475 Subread feature Counts v1.5.0-p1 [73]. Differentially expressed genes (DEGs) were
476 determined by DESeq2 v1.14.1 [73] using a false discory rate of 0.05. Ingenuity Pathway
477 Analysis (Qiagen) and Gene Set Enrichment Analysis v4.0.3 (GSEA) were further used
478 as previously described [74].

479

480 **Ultrahigh Performance Liquid Chromatography-Tandem Mass Spectroscopy**

481 Hepatocytes were isolated described above for metabolomic screening via Ultrahigh
482 Performance Liquid Chromotography-Tandem Mass Spectroscopy (UPLC-MS/MS)
483 (Metabolon; NC, USA). Briefly, 150-200 microliter cell pellets per animal were used as
484 starting material. Samples were prepared using the automated MicroLab STAR system
485 (Hamilton; NV, USA). Proteins were precipitated using methanol under vigorous shaking
486 for 2 minutes followed by centrifugation. Prior to analysis organic solvents were removed

487 with TurboVap (Zymark; MA, USA) and overnight storage under nitrogen. Dried samples
488 were reconstituted with solvents compatible with the three following analytical methods:
489 1) reverse phase (RP)/UPLC-MS/MS methods with positive ion mode electrospray
490 ionization (ESI), 2) RP/UPLC-MS/MS with negative ion mode ESI and 3) HILIC/UPLC-
491 MS/MS with negative ion mode ESI. Resulting samples were analyzed with the ACQUITY
492 UPLC (Waters; MA, USA) and a Q-Exactive high resolution/accurate mass spectrometer
493 (ThermoScientific; MA, USA) interfaced with a heated electrospray ionization (HESI-II)
494 source and Orbitrap mass analyzer operated at 35,000 mass resolution. An acidic positive
495 ion condition was used on an aliquot optimized to detect more hydrophilic compounds.
496 Another acidic positive ion condition was ran but chromotographically optimized for
497 hydrophobic compounds. Basic negative ion optimized conditions was also used on a
498 separate C18 column. Resulting raw data was extracted and peaks identified using
499 Metabolon's hardware and software. Compounds were identified by comnparing to known
500 library entries of purified standards or recurrent unknown entities. A lirary of authenticated
501 standards containing retention time/index (RI), mass to charge ratio (*m/z*) and
502 chromotographic data (MS/MS spectral data) on all library compounds. Three criteria are
503 used to identify chemicals: 1) RI within a narrow window of proposed identification, 2)
504 accurate mass match to the library ± 10 ppm and 3) MS/MS forward and reverse scores
505 between the experimental data and authentic standards. Peaks were quantified using
506 area under the curve (AUC). For complex lipid panel lipids were extracted with
507 methanol:dichloromethane in the presence of internal standards. Extracts were
508 concentrated under nitrogen and reconstituted in 250ml of 10mM ammonium acetate
509 dichloromethane:methanol (50:50). Mass spec analysis was performed in a Shimazdu LC

510 with nano PEEK tubing and the Sciex SlexIon-5500 QTRAP (Sciex; MA, USA). Both
511 negative and positive mode electrospray was used. Individual lipid species were
512 quantified by taking the peak area ratios of target compounds and their assigned internal
513 standards then multiplying by the concentration of added internal standards. Lipid class
514 concentrations were calculated from the sum of all molecular species within a class, and
515 fatty acid compositions were determined by calculating the proportion of each class
516 comprised by individual fatty acids.
517

518 **Oil Red O Staining**

519 Livers were frozen in optimal cutting temperature (OCT) media (FisherScientific; NH,
520 USA) and sectioned with a cryostat (Leica; Wetzler, Germany) at 4mm. Liver sections
521 were fixed at room temperature for 15 minutes with 4% paraformaldehyde followed by
522 washing three times with phosphate buffered saline (PBS). Liver sections were then
523 incubated with Oil Red O as previously described [74,75]. Liver sections were then washed
524 three times with PBS and cover slipped with Fluoroshield Mounting Media (Sigma).
525 Stained slides were visualized with a brightfield microscope (Nikon; NY, USA).
526

527 **Indirect Calorimetry**

528 To measure whole body energy expenditure in live animals, mice were housed
529 individually in metabolic chambers of PhenoMaster (Indirect calorimetry system; TSE
530 systems, Germany) and acclimatized for 3 days with free access to food and water. The
531 Energy expenditure (Oxygen consumption (VO2), Respiratory exchange ratio (RER) and

food intake were obtained continuously during a 12 h light and 12 h dark cycle for four days and measured for last 24 h after adaptation.

Acknowledgements

The authors of this manuscript would like to thank the National Institute of Environmental Health Sciences Epigenomics and DNA Sequencing Core for their help with RNA-sequencing and Dr. Sara Grimm for her analysis of transcriptome data. This work was supported by NIH Intramural Program 1ZIAES10328601 (J.M.), NIH R01 HL132035 (X.Z.), NIH K01 DK117069 (C.K), NIH K01 AG056663 (E.Q.), NIH R01 AI065791 (C.E.M.), R01 GM102497 (C.E.M.), R35 GM126922 (C.E.M.).

Citations

1 Buchman, T. G. *et al.* Sepsis Among Medicare Beneficiaries: 1. The Burdens of Sepsis, 2012–2018. *Critical Care Medicine* **48**, 276 (2020).

2 Rhee, C. *et al.* Incidence and trends of sepsis in US hospitals using clinical vs claims data, 2009-2014. *Jama* **318**, 1241-1249 (2017).

3 Mira, J. C. *et al.* Sepsis Pathophysiology, Chronic Critical Illness, and Persistent Inflammation-Immunosuppression and Catabolism Syndrome. *Crit Care Med* **45**, 253-262, doi:10.1097/CCM.0000000000002074 (2017).

4 Vachharajani, V. & McCall, C. E. Epigenetic and metabolic programming of innate immunity in sepsis. *Innate Immun* **25**, 267-279, doi:10.1177/1753425919842320 (2019).

5 Netea, M. G. *et al.* Defining trained immunity and its role in health and disease. *Nat Rev Immunol* **20**, 375-388, doi:10.1038/s41577-020-0285-6 (2020).

6 Lewis, A. J., Billiar, T. R. & Rosengart, M. R. Biology and metabolism of sepsis: innate immunity, bioenergetics, and autophagy. *Surgical infections* **17**, 286-293 (2016).

7 Bermudes, A. C. G. *et al.* Changes in lipid metabolism in pediatric patients with severe sepsis and septic shock. *Nutrition* **47**, 104-109 (2018).

8 Cheng, S.-C. *et al.* Broad defects in the energy metabolism of leukocytes underlie immunoparalysis in sepsis. *Nature immunology* **17**, 406 (2016).

9 Singer, M. The role of mitochondrial dysfunction in sepsis-induced multi-organ failure. *Virulence* **5**, 66-72 (2014).

10 Druml, W., Heinzel, G. & Kleinberger, G. Amino acid kinetics in patients with sepsis. *The American journal of clinical nutrition* **73**, 908-913 (2001).

11 Mecatti, G. C., Messias, M. C. F. & de Oliveira Carvalho, P. Lipidomic profile and candidate biomarkers in septic patients. *Lipids in Health and Disease* **19**, 1-9 (2020).

12 Quinones, Q. J., Ma, Q., Zhang, Z., Barnes, B. M. & Podgoreanu, M. V. Organ protective mechanisms common to extremes of physiology: a window through hibernation biology. *American Zoologist* **54**, 497-515 (2014).

13 Singer, M. *et al.* The Third International Consensus Definitions for Sepsis and Septic Shock (Sepsis-3). *JAMA* **315**, 801-810, doi:10.1001/jama.2016.0287 (2016).

14 Stacpoole, P. W. The pyruvate dehydrogenase complex as a therapeutic target for age-related diseases. *Aging cell* **11**, 371-377 (2012).

15 McCall, C. E. *et al.* Pyruvate dehydrogenase complex stimulation promotes immunometabolic homeostasis and sepsis survival. *JCI insight* **3** (2018).

16 Zhu, X. *et al.* Stimulating pyruvate dehydrogenase complex reduces itaconate levels and enhances TCA cycle anabolic bioenergetics in acutely inflamed monocytes. *J Leukoc Biol* **107**, 467-484, doi:10.1002/JLB.3A1119-236R (2020).

17 Dahn, M. S., Mitchell, R. A., Lange, M. P., Smith, S. & Jacobs, L. A. Hepatic metabolic response to injury and sepsis. *Surgery* **117**, 520-530 (1995).

18 Liu, P. S. *et al.* alpha-ketoglutarate orchestrates macrophage activation through metabolic and epigenetic reprogramming. *Nat Immunol* **18**, 985-994, doi:10.1038/ni.3796 (2017).

19 Mills, E. & O'Neill, L. A. Succinate: a metabolic signal in inflammation. *Trends Cell Biol* **24**, 313-320, doi:10.1016/j.tcb.2013.11.008 (2014).

20 Mills, E. L. *et al.* Succinate Dehydrogenase Supports Metabolic Repurposing of Mitochondria to Drive Inflammatory Macrophages. *Cell* **167**, 457-470 e413, doi:10.1016/j.cell.2016.08.064 (2016).

613 21 Lampropoulou, V. *et al.* Itaconate Links Inhibition of Succinate Dehydrogenase with Macrophage
614 Metabolic Remodeling and Regulation of Inflammation. *Cell Metab* **24**, 158-166,
615 doi:10.1016/j.cmet.2016.06.004 (2016).
616 22 Liao, S. T. *et al.* 4-Octyl itaconate inhibits aerobic glycolysis by targeting GAPDH to exert anti-
617 inflammatory effects. *Nat Commun* **10**, 5091, doi:10.1038/s41467-019-13078-5 (2019).
618 23 Mills, E. L. *et al.* Itaconate is an anti-inflammatory metabolite that activates Nrf2 via alkylation of
619 KEAP1. *Nature* **556**, 113-117, doi:10.1038/nature25986 (2018).
620 24 Daniels, B. P. *et al.* The Nucleotide Sensor ZBP1 and Kinase RIPK3 Induce the Enzyme IRG1 to
621 Promote an Antiviral Metabolic State in Neurons. *Immunity* **50**, 64-76 e64,
622 doi:10.1016/j.immuni.2018.11.017 (2019).
623 25 Indo, H. P. *et al.* Evidence of ROS generation by mitochondria in cells with impaired electron
624 transport chain and mitochondrial DNA damage. *Mitochondrion* **7**, 106-118,
625 doi:10.1016/j.mito.2006.11.026 (2007).
626 26 Simoes, I. C. M., Fontes, A., Pinton, P., Zischka, H. & Wieckowski, M. R. Mitochondria in non-
627 alcoholic fatty liver disease. *Int J Biochem Cell Biol* **95**, 93-99, doi:10.1016/j.biocel.2017.12.019
628 (2018).
629 27 Brooks, H., Osabutey, C., Moss, R., Andrews, P. & Davies, D. Caecal ligation and puncture in the
630 rat mimics the pathophysiological changes in human sepsis and causes multi-organ dysfunction.
631 *Metabolic brain disease* **22**, 353-373 (2007).
632 28 Okin, D. & Medzhitov, R. Evolution of inflammatory diseases. *Curr Biol* **22**, R733-740,
633 doi:10.1016/j.cub.2012.07.029 (2012).
634 29 Weis, S. *et al.* Metabolic Adaptation Establishes Disease Tolerance to Sepsis. *Cell* **169**, 1263-1275
635 e1214, doi:10.1016/j.cell.2017.05.031 (2017).
636 30 Quinn, M. A. & Cidlowski, J. A. Endogenous hepatic glucocorticoid receptor signaling coordinates
637 sex-biased inflammatory gene expression. *FASEB J*, doi:10.1096/fj.15-278309 (2015).
638 31 Dąbek, A., Wojtala, M., Pirola, L. & Balcerczyk, A. Modulation of Cellular Biochemistry,
639 Epigenetics and Metabolomics by Ketone Bodies. Implications of the Ketogenic Diet in the
640 Physiology of the Organism and Pathological States. *Nutrients* **12**, 788 (2020).
641 32 DiMarco, N. M., Beitz, D. C. & Whitehurst, G. B. Effect of fasting on free fatty acid, glycerol and
642 cholesterol concentrations in blood plasma and lipoprotein lipase activity in adipose tissue of
643 cattle. *J Anim Sci* **52**, 75-82, doi:10.2527/jas1981.52175x (1981).
644 33 McCall, C. E. *et al.* Pyruvate dehydrogenase complex stimulation promotes immunometabolic
645 homeostasis and sepsis survival. *JCI Insight* **3**, doi:10.1172/jci.insight.99292 (2018).
646 34 Breuille, D. *et al.* A sustained rat model for studying the long-lasting catabolic state of sepsis.
647 *Infect Immun* **67**, 1079-1085 (1999).
648 35 Laudanski, K. *et al.* The clinical and immunological performance of 28 days survival model of
649 cecal ligation and puncture in humanized mice. *PLoS One* **12**, e0180377,
650 doi:10.1371/journal.pone.0180377 (2017).
651 36 Pugh, A. M., Auteri, N. J., Goetzman, H. S., Caldwell, C. C. & Nomellini, V. A Murine Model of
652 Persistent Inflammation, Immune Suppression, and Catabolism Syndrome. *Int J Mol Sci* **18**,
653 doi:10.3390/ijms18081741 (2017).
654 37 Buck, M. D., Sowell, R. T., Kaech, S. M. & Pearce, E. L. Metabolic Instruction of Immunity. *Cell*
655 **169**, 570-586, doi:10.1016/j.cell.2017.04.004 (2017).
656 38 Williams, N. C. & O'Neill, L. A. A role for the Krebs cycle intermediate citrate in metabolic
657 reprogramming in innate immunity and inflammation. *Frontiers in immunology* **9**, 141 (2018).
658 39 Zaslona, Z. & O'Neill, L. A. J. Cytokine-like Roles for Metabolites in Immunity. *Mol Cell*,
659 doi:10.1016/j.molcel.2020.04.002 (2020).

40 McGuire, V. A. *et al.* Dimethyl fumarate blocks pro-inflammatory cytokine production via inhibition of TLR induced M1 and K63 ubiquitin chain formation. *Scientific reports* **6**, 31159 (2016).
41 Della Giustina, A. *et al.* Dimethyl fumarate modulates oxidative stress and inflammation in organs after Sepsis in rats. *Inflammation* **41**, 315-327 (2018).
42 Qin, W. *et al.* S-glycosylation-based cysteine profiling reveals regulation of glycolysis by itaconate. *Nat Chem Biol* **15**, 983-991, doi:10.1038/s41589-019-0323-5 (2019).
43 Bambouskova, M. *et al.* Electrophilic properties of itaconate and derivatives regulate the IκBζ–ATF3 inflammatory axis. *Nature* **556**, 501-504 (2018).
44 Hooftman, A. & O'Neill, L. A. The immunomodulatory potential of the metabolite itaconate. *Trends in immunology* (2019).
45 Yi, Z. *et al.* IRG1/Itaconate Activates Nrf2 in Hepatocytes to Protect Against Liver Ischemia-Reperfusion Injury. *Hepatology*, doi:10.1002/hep.31147 (2020).
46 Giustina, A. D. *et al.* Vitamin B6 reduces oxidative stress in lungs and liver in experimental sepsis. *An Acad Bras Cienc* **91**, e20190434, doi:10.1590/0001-3765201920190434 (2019).
47 Chen, J. *et al.* Protective effects of melatonin on sepsis-induced liver injury and dysregulation of gluconeogenesis in rats through activating SIRT1/STAT3 pathway. *Biomed Pharmacother* **117**, 109150, doi:10.1016/j.biopha.2019.109150 (2019).
48 Langley, R. J. *et al.* An integrated clinico-metabolomic model improves prediction of death in sepsis. *Sci Transl Med* **5**, 195ra195, doi:10.1126/scitranslmed.3005893 (2013).
49 Liu, T. F., Vachharajani, V. T., Yoza, B. K. & McCall, C. E. NAD+-dependent sirtuin 1 and 6 proteins coordinate a switch from glucose to fatty acid oxidation during the acute inflammatory response. *Journal of biological chemistry* **287**, 25758-25769 (2012).
50 Galván-Peña, S. *et al.* Malonylation of GAPDH is an inflammatory signal in macrophages. *Nature communications* **10**, 1-11 (2019).
51 Galvan-Pena, S. *et al.* Malonylation of GAPDH is an inflammatory signal in macrophages. *Nat Commun* **10**, 338, doi:10.1038/s41467-018-08187-6 (2019).
52 Koskinas, J. *et al.* Liver histology in ICU patients dying from sepsis: a clinico-pathological study. *World journal of gastroenterology: WJG* **14**, 1389 (2008).
53 Balasse, E. O. & Féry, F. Ketone body production and disposal: effects of fasting, diabetes, and exercise. *Diabetes/metabolism reviews* **5**, 247-270 (1989).
54 Newman, J. C. & Verdin, E. Ketone bodies as signaling metabolites. *Trends in Endocrinology & Metabolism* **25**, 42-52 (2014).
55 OWEN, O. E. & Schramm, V. L. (Portland Press Ltd., 1981).
56 Barcellos, L., Marqueze, A., Trapp, M., Quevedo, R. & Ferreira, D. The effects of fasting on cortisol, blood glucose and liver and muscle glycogen in adult jundiá Rhamdia quelen. *Aquaculture* **300**, 231-236 (2010).
57 Nakamura, K. *et al.* Effect of food-restriction stress on immune response in mice. *Journal of neuroimmunology* **30**, 23-29 (1990).
58 Xu, C. *et al.* Direct effect of glucocorticoids on lipolysis in adipocytes. *Molecular endocrinology* **23**, 1161-1170 (2009).
59 Zhu, X. *et al.* Stimulating pyruvate dehydrogenase complex reduces itaconate levels and enhances TCA cycle anabolic bioenergetics in acutely inflamed monocytes. *Journal of Leukocyte Biology* (2020).
60 Min, B. K. *et al.* Pyruvate Dehydrogenase Kinase Is a Metabolic Checkpoint for Polarization of Macrophages to the M1 Phenotype. *Front Immunol* **10**, 944, doi:10.3389/fimmu.2019.00944 (2019).

707 61 Huang, B., Wu, P., Bowker-Kinley, M. M. & Harris, R. A. Regulation of pyruvate dehydrogenase
708 kinase expression by peroxisome proliferator-activated receptor-alpha ligands, glucocorticoids,
709 and insulin. *Diabetes* **51**, 276-283, doi:10.2337/diabetes.51.2.276 (2002).
710 62 Hutson, N. J. & Randle, P. J. Enhanced activity of pyruvate dehydrogenase kinase in rat heart
711 mitochondria in alloxan-diabetes or starvation. *FEBS Lett* **92**, 73-76, doi:10.1016/0014-
712 5793(78)80724-8 (1978).
713 63 Baxter, M. A. & Coore, H. G. The mode of regulation of pyruvate dehydrogenase of lactating rat
714 mammary gland. Effects of starvation and insulin. *Biochem J* **174**, 553-561,
715 doi:10.1042/bj1740553 (1978).
716 64 Fuller, S. J. & Randle, P. J. Reversible phosphorylation of pyruvate dehydrogenase in rat skeletal-
717 muscle mitochondria. Effects of starvation and diabetes. *Biochem J* **219**, 635-646,
718 doi:10.1042/bj2190635 (1984).
719 65 Denyer, G. S., Kerbey, A. L. & Randle, P. J. Kinase activator protein mediates longer-term effects
720 of starvation on activity of pyruvate dehydrogenase kinase in rat liver mitochondria. *Biochem J*
721 **239**, 347-354, doi:10.1042/bj2390347 (1986).
722 66 Wu, P. *et al.* Starvation increases the amount of pyruvate dehydrogenase kinase in several
723 mammalian tissues. *Arch Biochem Biophys* **381**, 1-7, doi:10.1006/abbi.2000.1946 (2000).
724 67 Klyuyeva, A., Tuganova, A., Kedishvili, N. & Popov, K. M. Tissue-specific kinase expression and
725 activity regulate flux through the pyruvate dehydrogenase complex. *J Biol Chem* **294**, 838-851,
726 doi:10.1074/jbc.RA118.006433 (2019).
727 68 Bao, H., Kasten, S. A., Yan, X. & Roche, T. E. Pyruvate dehydrogenase kinase isoform 2 activity
728 limited and further inhibited by slowing down the rate of dissociation of ADP. *Biochemistry* **43**,
729 13432-13441, doi:10.1021/bi049488x (2004).
730 69 Pratt, M. L. & Roche, T. E. Mechanism of pyruvate inhibition of kidney pyruvate dehydrogenasea
731 kinase and synergistic inhibition by pyruvate and ADP. *J Biol Chem* **254**, 7191-7196 (1979).
732 70 Vachharajani, V. T. *et al.* SIRT1 inhibition during the hypoinflammatory phenotype of sepsis
733 enhances immunity and improves outcome. *J Leukoc Biol* **96**, 785-796,
734 doi:10.1189/jlb.3MA0114-034RR (2014).
735 71 Chen, Z., Fitzgerald, R. L., Averna, M. R. & Schonfeld, G. A targeted apolipoprotein B-38.9-
736 producing mutation causes fatty livers in mice due to the reduced ability of apolipoprotein B-
737 38.9 to transport triglycerides. *J Biol Chem* **275**, 32807-32815, doi:10.1074/jbc.M004913200
738 (2000).
739 72 Dobin, A. *et al.* STAR: ultrafast universal RNA-seq aligner. *Bioinformatics* **29**, 15-21,
740 doi:10.1093/bioinformatics/bts635 (2013).
741 73 Liao, Y., Smyth, G. K. & Shi, W. featureCounts: an efficient general purpose program for
742 assigning sequence reads to genomic features. *Bioinformatics* **30**, 923-930,
743 doi:10.1093/bioinformatics/btt656 (2014).
744 74 Quinn, M. A., Xu, X., Ronfani, M. & Cidlowski, J. A. Estrogen Deficiency Promotes Hepatic
745 Steatosis via a Glucocorticoid Receptor-Dependent Mechanism in Mice. *Cell Rep* **22**, 2690-2701,
746 doi:10.1016/j.celrep.2018.02.041 (2018).
747 75 Mehlem, A., Hagberg, C. E., Muhl, L., Eriksson, U. & Falkevall, A. Imaging of neutral lipids by oil
748 red O for analyzing the metabolic status in health and disease. *Nat Protoc* **8**, 1149-1154,
749 doi:10.1038/nprot.2013.055 (2013).

750

751

752 **Figure Legends**

753 **Figure 1: Sepsis Impairs hepatic mitochondrial metabolism.** (A) Top 5 canonical
754 pathways subject to transcriptional alterations in the liver identified by Ingenuity Pathway
755 Analysis of RNA-seq of sham versus CLP mice (n = 4 mice per group). Blue represents
756 a negative z-score and orange represents a positive z-score. Shading indicates intensity
757 of pathway activation/inhibition. (B) GSEA of the oxidative phosphorylation pathway
758 (GO:0006119) indicating a negative normalized enrichment score (NES = -0.853). (C)
759 GSEA of the TCA cycle pathway (GO:0006099) indicating a negative enrichment score
760 (NES = -1.1956). (D) Schematic representation of hepatic TCA cycle metabolites altered
761 during chronic sepsis. Red denotes a metabolite increased in response to sepsis; green
762 indicates a metabolite decreased in response to sepsis; black indicates a metabolite un-
763 changed in response to sepsis; grey indicates a metabolite not measured in our metabo-
764 lomic screening. (E-J) Relative metabolite levels measured by Ultrahigh Performance Liq-
765 uid Chromatography-Tandem Mass Spectroscopy (UPLC-MS/MS) from livers of sham
766 and CLP mice 30 hours post-surgery (n = 5 sham; 8 CLP). (K) rlog transformed counts
767 from RNA-seq of sham and CLP mice 30 hours post-surgery. (L) Relative itaconate levels
768 in livers of sham and CLP mice measured by UPLC-MS/MS (n = 5 sham; 8 CLP). * de-
769 notes $p<0.05$.

770

771 **Figure 2: Impaired hepatic redox balance in septic mice.** (A) GSEA of the ROS met-
772 abolic pathway (GO:0072593) from RNA-seq from livers comparing sham to CLP showing
773 a positive enrichment score (NES = 1.117) (n = 4 mice per group). (B-F) Relative metab-
774 olite levels of metabolites involved in redox balance measured by UPLC-MS/MS (n = 5

775 sham; 8 CLP). (G) % of glutathione pool that is either oxidized or reduced in livers from
776 sham and CLP mice 30 hours post-surgery. * denotes $p<0.05$, **** $p<0.0001$.

777

778 **Figure 3: Sepsis promotes hepatic steatosis.** (A) Top 5 induced and repressed physi-
779 ological pathways in the liver of sham versus CLP mice identified by IPA of RNA-seq. (B)
780 GSEA of the fatty acid metabolic pathway (GO:0019395) from RNA-seq from livers com-
781 paring sham to CLP showing a negative enrichment score (NES = -1.018) (n = 4 mice per
782 group). (C) Heatmap representation of average log2 fold change of genes involved in fatty
783 acid oxidation (GO:0019395) and fatty acid biosynthetic process (GO:0006633) in CLP
784 versus sham operated mice (n = 5 sham; n = 8 CLP). (D) IPA of top 5 metabolic pathways
785 significantly altered in the liver in response to sepsis identified by global metabolomic
786 screening. (E) Heatmap representation of log2 fold change of different lipid species in
787 sham and CLP mice measured by UPLC-MS/MS. (F) Targeted lipidomic screening by
788 UPLC-MS/MS of livers from sham and CLP mice 30 hours post-surgery (n = 5 sham; n =
789 8 CLP). (G) Oil red O staining of frozen liver sections from sham and CLP mice 30 hours
790 post-surgery. Scale bar is 50μm. Image is representative of 3 independent mice per
791 group.

792

793 **Figure 4: Sepsis-induced anorexia increases plasma free fatty acid levels.** (A) Cu-
794 mulative food intake over 24-hour period following sham or CLP surgery. (B) Relative
795 abundance of (B) glucose, (C) corticosterone, (D) 3-hydroxybutyrate, (E) 2-hydroxybutyr-
796 ate and (F) 2-aminobutyrate measured by UPLC-MS/MS in plasma from sham and CLP

797 mice 30 hours post-surgery (n = 6 sham; n = 10 CLP). (G) Heatmap representation of fold
798 change of different lipid species in plasma from sham and CLP mice 30 hours post-sur-
799 gery (n = 6 sham; n = 10 CLP). * denotes p<0.05, ** p<0.01, p<0.001, **** p<0.0001.

800

801 **Figure 5: PDK inhibition restores hepatic metabolism in septic mice.** (A) Venn dia-
802 gram of differentially expressed genes (DEGs) assessed by RNA-seq in CLP versus
803 sham compared to CLP+DCA versus sham 30 hours post-surgery (left). Heatmap of av-
804 erage log2 fold change of DEGs in sham, CLP and CLP+DCA (right) (n = 4 mice per
805 group). (B) Heatmap depiction of z-scores of top canonical pathways identified by IPA in
806 CLP versus sham and CLP+DCA versus sham. (C) Heatmap depiction of average log2
807 fold change in metabolite levels involved in TCA cycle in sham, CLP and CLP+DCA 30
808 hours post-surgery measured by UPLC-MS/MS (n = 5 sham; n = 8 CLP and CLP+DCA).
809 (D) Heatmap depiction of average log2 fold change in metabolite levels involved in redox
810 balance in sham, CLP and CLP+DCA 24 hours post-surgery measured by UPLC-MS/MS
811 (n = 5 sham; n = 8 CLP and CLP+DCA). (E) GSSG/GSH ratio in sham, CLP and
812 CLP+DCA measured by UPLC-MS/MS. (F) Average fold change in monoacylglycerol,
813 diacylglycerol and triacylglycerol in CLP and CLP+DCA relative to sham measured by
814 UPLC-MS/MS. (G) Oil red O staining of frozen liver sections from sham and CLP mice 30
815 hours post-surgery. Scale bar is 50μm * denotes p<0.05, ** p<0.01, *** p<0.001, ****
816 p<0.0001.

817

818 **Figure 6: DCA rescues systemic energy crisis during polymicrobial infection.** (A)
819 Heatmap of average log2 fold change in plasma metabolite levels in sham, CLP and
820 CLP+DCA (left) assessed by UPLC-MS/MS. Venn diagram of altered plasma metabolites
821 in CLP versus sham compared to CLP+DCA versus sham 30 hours post-surgery (right)
822 (n = 6 sham; n = 10 CLP and CLP+DCA). (C) Pathway analysis of 198 unique plasma
823 metabolites altered in CLP mice. Left: % overlap of metabolites changed in CLP mice with
824 metabolic pathway. Right: -log(p-value) of pathways altered. (D) Change in body weight
825 in sham, CLP and CLP+DCA 30 hours post-surgery. Total food intake after 30 hours post-
826 surgery in sham, CLP and CLP+DCA. (F) Respiratory exchange ratio (RER) in VO2 in
827 sham, CLP and CLP+DCA 24 hours-post surgery. (H) Schematic representation of he-
828 patic and systemic energy consequences of sepsis and PDK inhibition. * denotes $p<0.05$,
829 ** $p<0.01$, *** $p<0.001$.

830

831

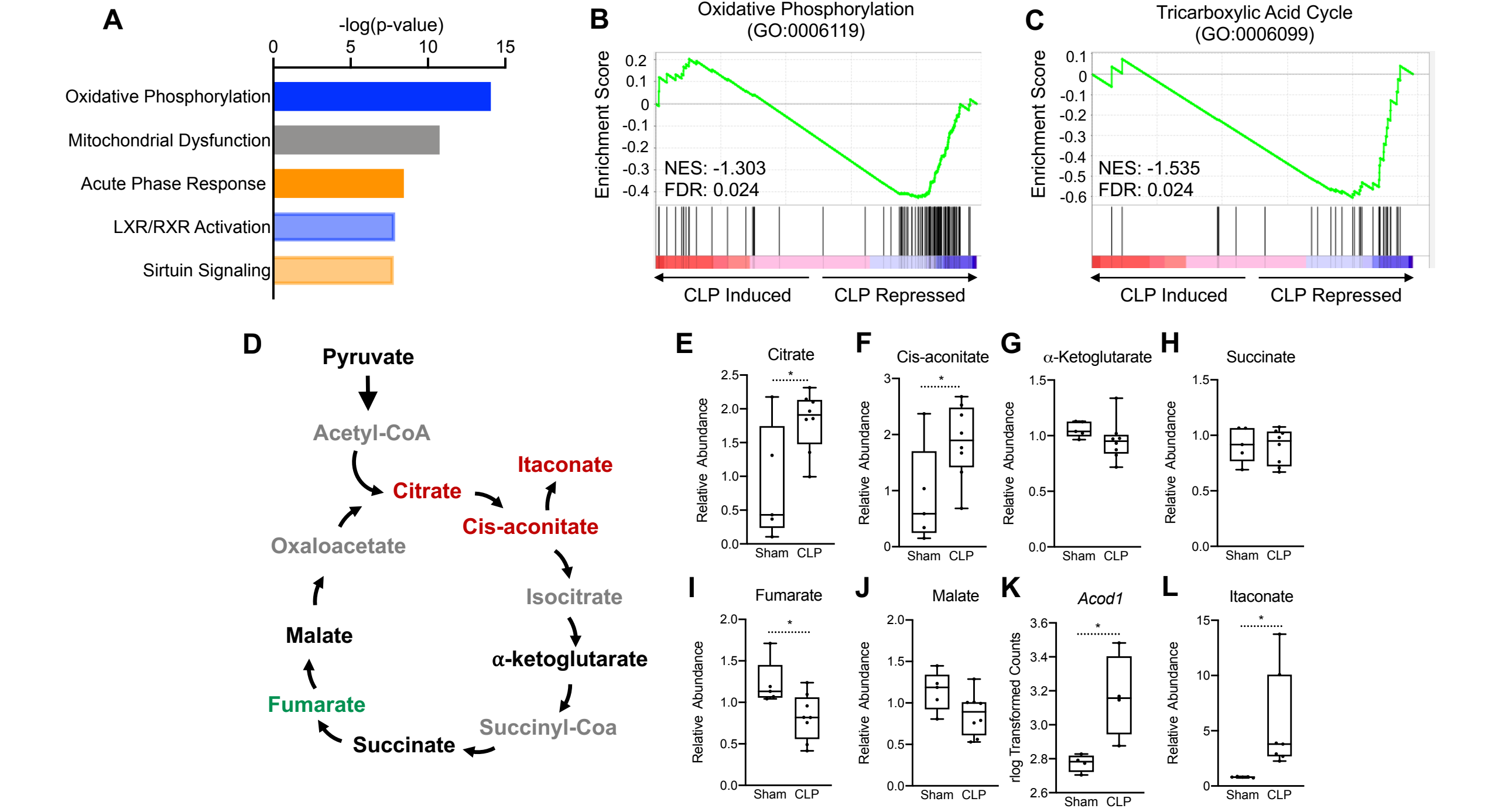

Figure 1: Sepsis Impairs Hepatic Mitochondrial Metabolism

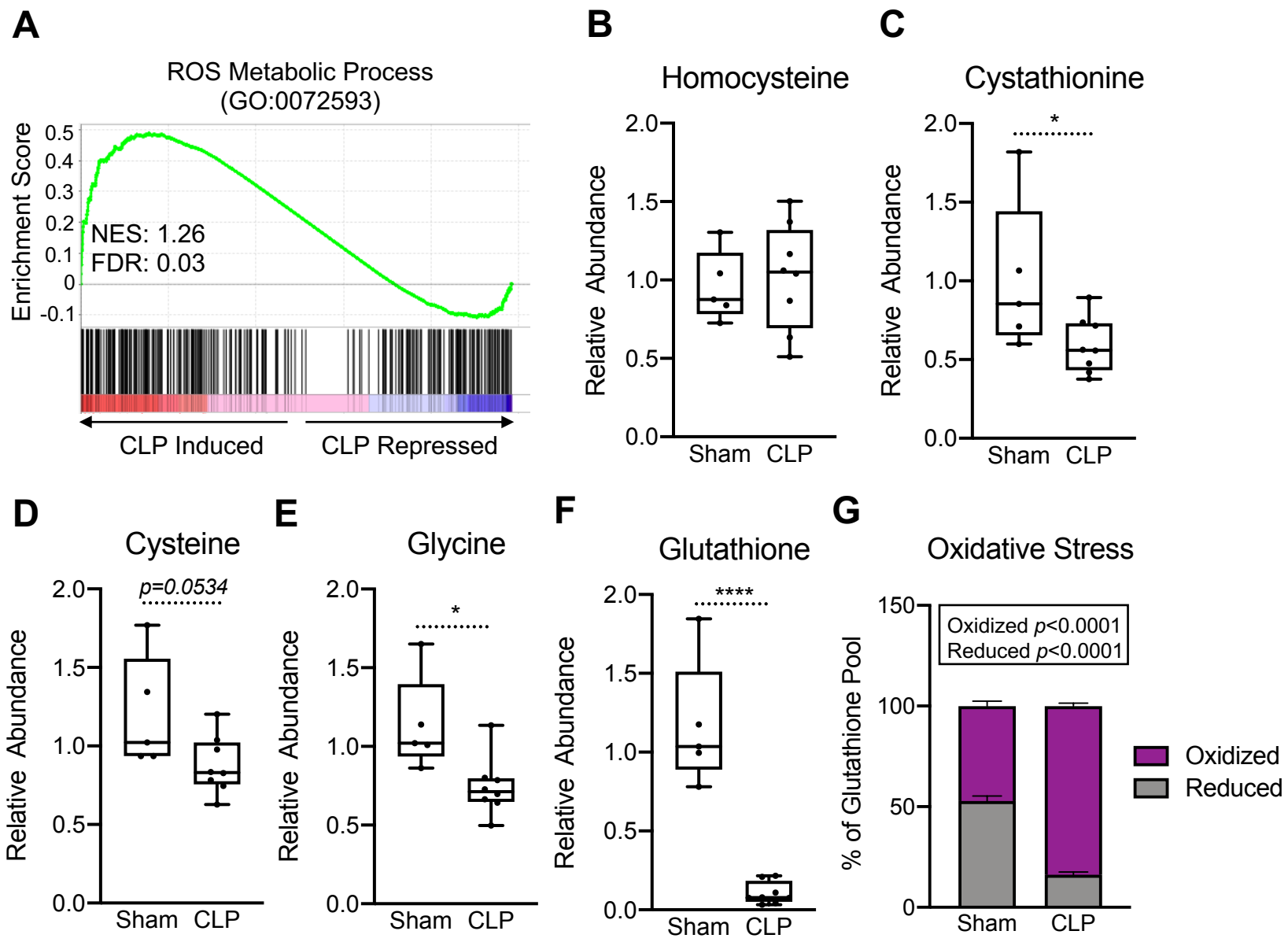

Figure 2: Impaired Hepatic Redox Balance in Septic Mice

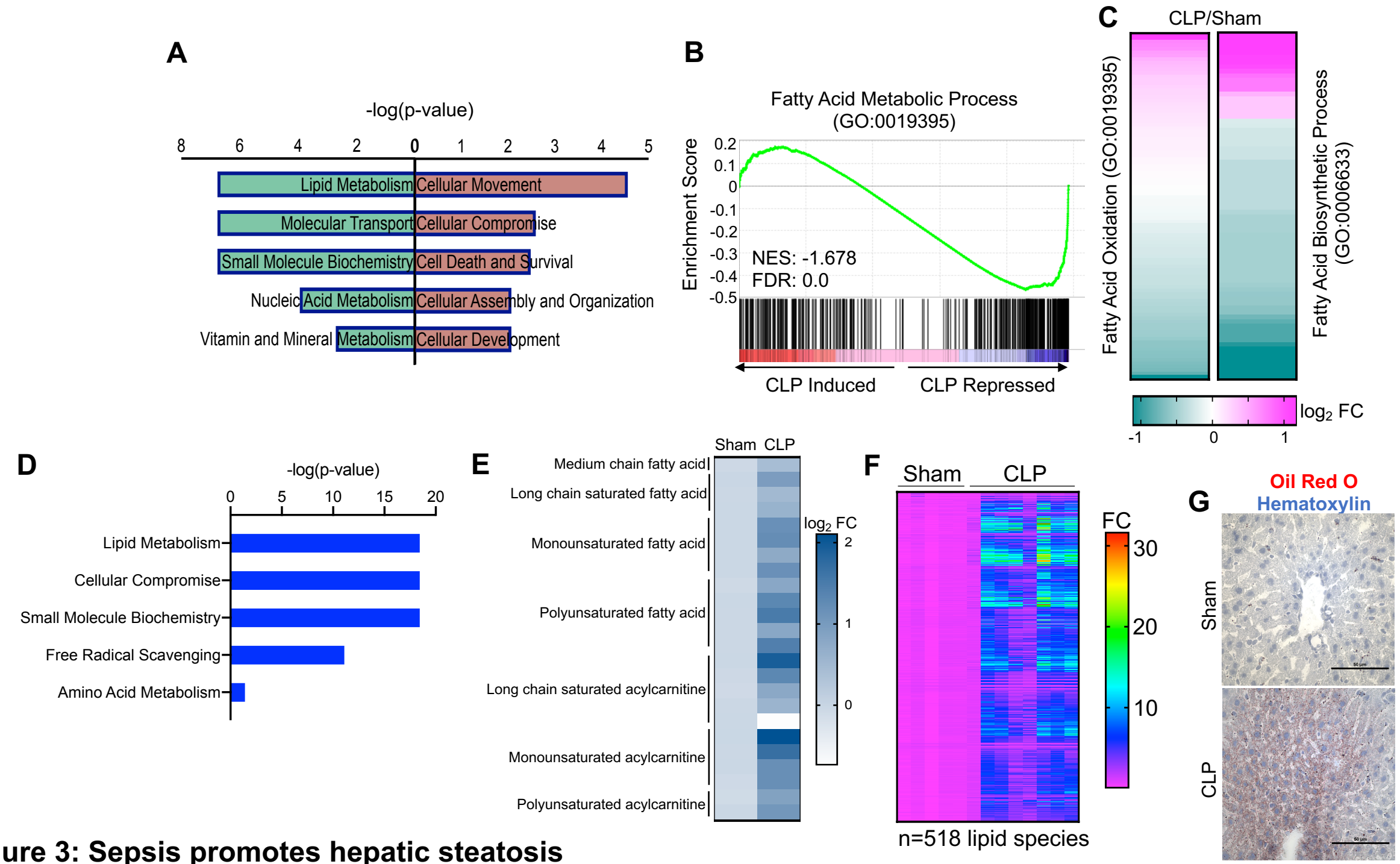

Figure 3: Sepsis promotes hepatic steatosis

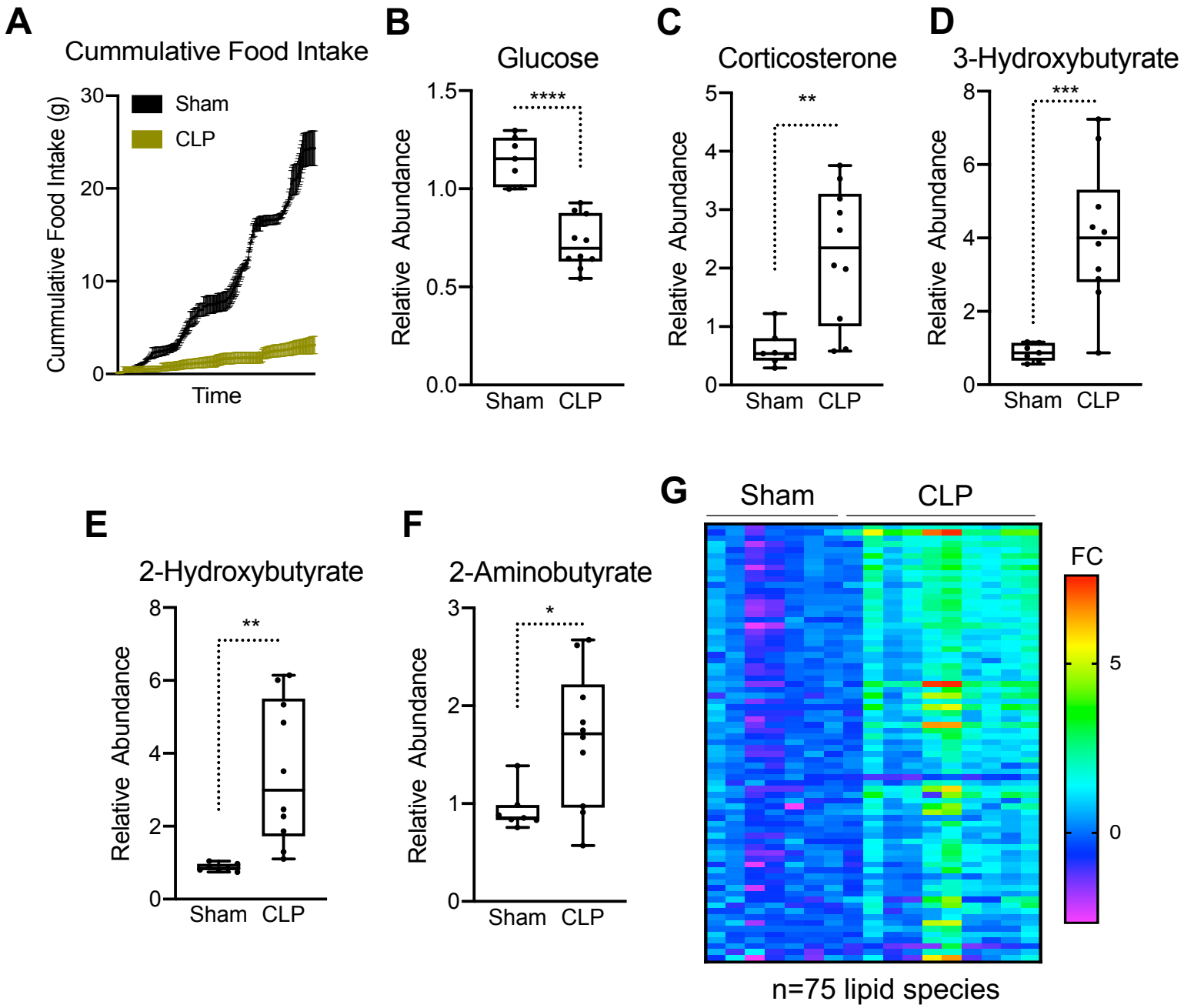

Figure 4: : Sepsis-induced anorexia increases plasma free fatty acid levels

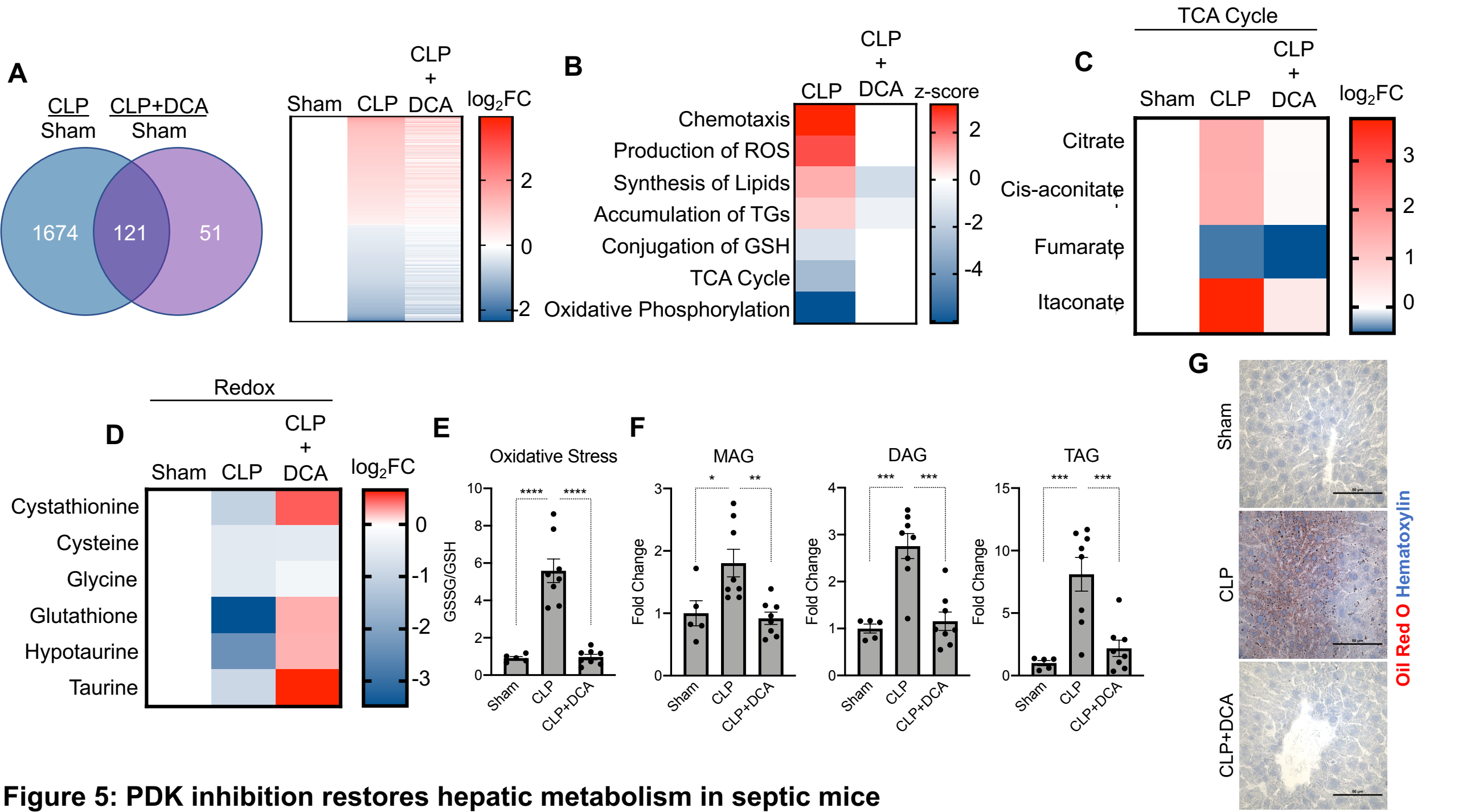

Figure 5: PDK inhibition restores hepatic metabolism in septic mice

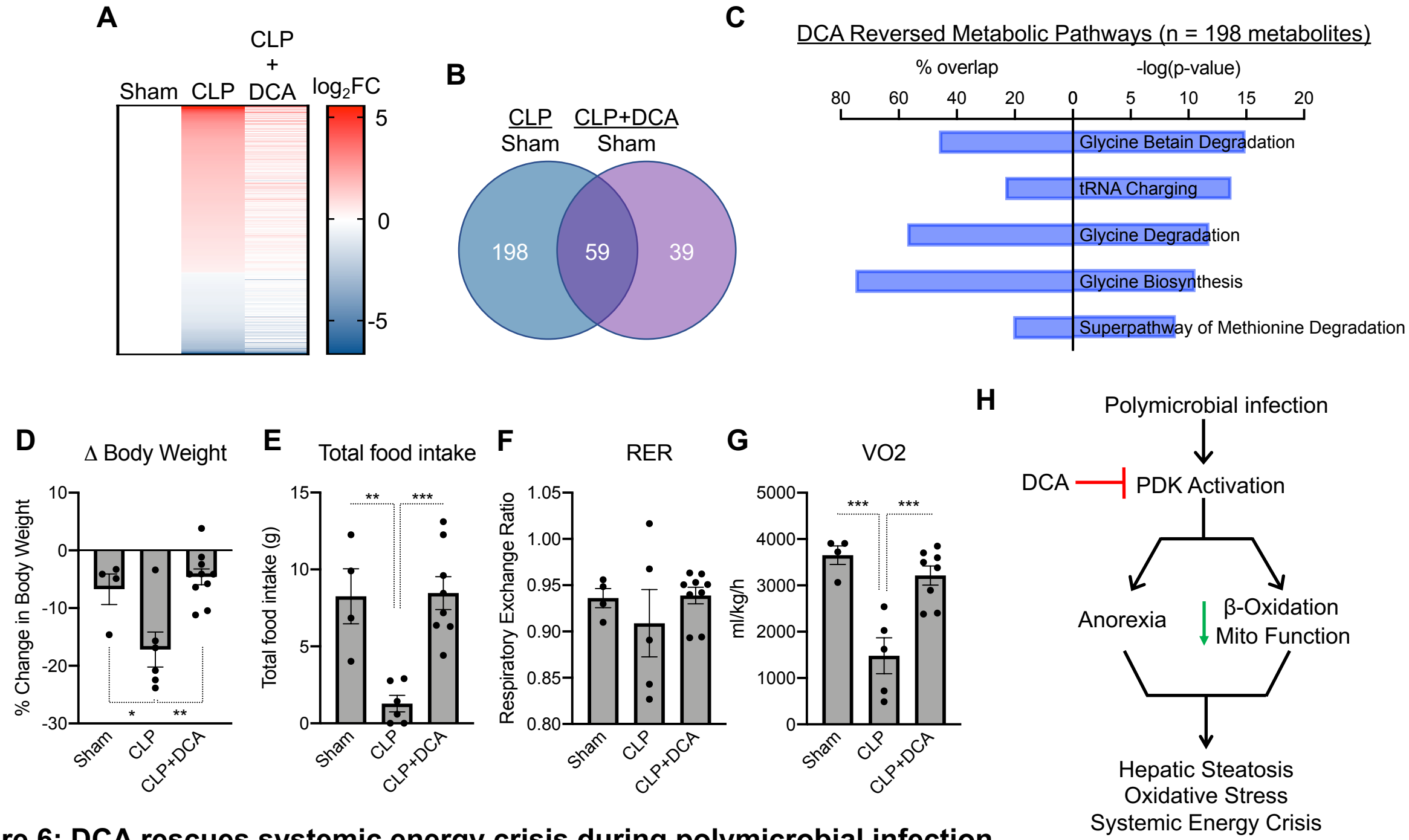

Figure 6: DCA rescues systemic energy crisis during polymicrobial infection